THE ASTROPHYSICAL JOURNAL, **211**:160–169, 1977 January 1

VERY LONG BASELINE INTERFEROMETRIC OBSERVATIONS OF OH MASERS ASSOCIATED WITH INFRARED STARS

J. M. MORAN AND J. A. BALL
Center for Astrophysics, Harvard College Observatory and Smithsonian Astrophysical Observatory
J. L. YEN
Electrical Engineering Department, University of Toronto
AND
P. R. SCHWARTZ, K. J. JOHNSTON, AND S. H. KNOWLES
E. O. Hulburt Center for Space Research, Naval Research Laboratory

Received 1976 April 28

ABSTRACT

Interferometric observations of 12 OH/IR sources at 1612 MHz were made on a baseline having a minimum fringe spacing of 0".045. IRC +10011, IRC +50137, OH 1735−32, OH 1821−12, OH 1837−05, OH 1854+02, R Aql, and IRC −20540 produced no interference fringes, so the individual features in these sources were presumed to be larger than 0".06. Fringes on the sources VY CMa, VX Sgr, W43 A, and NML Cyg were seen and maps of their principal features produced. All the features in these sources had fringe visibilities of less than 0.3, except for one feature in VY CMa that was unresolved. The brightness temperatures of the features were typically 10^{10} K. Attempts were made to understand the geometry of the distribution of the maser emission in terms of an expanding spherical shell model.

Subject headings: infrared: sources — interferometry — stars: circumstellar shells — stars: long-period variables — stars: supergiants

I. INTRODUCTION

OH emission from infrared stars, both M supergiants and long-period variables, has been studied by Wilson and Barrett (1972); Wilson, Barrett, and Moran (1970); P. M. Harvey *et al.* (1974); Davies, Masheder, and Booth (1972); Masheder, Booth, and Davies (1974); and Reid and Muhleman (1975). The emission is generally unpolarized and occurs principally in the 1612 MHz satellite transition in two well-defined velocity ranges. In long-period variables, the structure of the spectra is usually simple, consisting of a few features, while in the supergiants the spectra contain tens to hundreds of features. A very long baseline interferometer (VLBI) experiment was conceived principally to examine the long-period variables in the hope that their angular structure would be understandable in terms of simple models.

II. OBSERVATIONS

The observations were made on 1973 April 6, 7, and 8, with a two-element VLBI. One element was the 150 foot (45.7 m) antenna of the Algonquin Radio Observatory, located in Algonquin Park, Ontario, Canada. The receiver was a room-temperature parametric amplifier which had a system temperature of 300 K. The hydrogen maser frequency standard used to generate the local oscillator at this station was not operating well, because of contamination in the discharge cavity. Consequently, the short-term frequency stability was adequate for the experiment, but the long-term stability was poor. This prevented us from measuring accurately the absolute positions of the sources. The second element was the 140 foot (42.7 m) antenna of the National Radio Astronomy Observatory (NRAO)[1] in Green Bank, West Virginia. The receiver there contained a cooled parametric amplifier, and the system temperature was 70 K. The local oscillator was phase-locked to a hydrogen maser frequency standard. Both stations received right-circular polarization. The data were recorded on the NRAO Mark II recording system.

The baseline had a length of 847 km, a declination of −46°, and an hour angle of 23ʰ1 measured from Algonquin Park. The minimum fringe spacing was 0".045. Because of the nearly north-south orientation, there was no appreciable foreshortening of the baseline, which would have been desirable for this experiment.

About 30 hours of data were recorded on 12 OH sources and two quasars used for delay calibration. Each observation lasted 30 minutes and included 25 minutes ON the source and 5 minutes OFF the source. The OFF-source part provided the bandpass needed for the single-antenna or total-power spectra. Data were taken on the sources VX Sgr, VY CMa, and NML Cyg with a 500 kHz bandwidth; and on W43 A, IRC +10011, IRC +50137, OH 1735−32, OH 1821 −12, OH 1837−05, OH 1854+02, R Aql, and IRC

---

[1] The National Radio Astronomy Observatory is operated by Associated Universities, Inc., under contract with the National Science Foundation.

−20540 with a 250 kHz bandwidth. Approximately four observations were made of each source.

III. DATA ANALYSIS

The data were processed through the NRAO Mark II VLB processor and its 96-channel correlator (Clark 1973). The correlation functions produced by the processor were analyzed by a series of programs on the IBM 360 general-purpose computer at NRAO (Moran 1973). The basic operations were the Fourier transform of the cross-correlation functions with respect to time and delay to obtain cross-power spectra as a function of fringe frequency and frequency or Doppler velocity. The spectral resolution, dictated by the 96-channel capability of the correlator and Hanning weighting in the Fourier transform, was 10.4 kHz or 1.9 km s^{-1} for the 250 kHz bandwidth, and 20.8 kHz or 3.9 km s^{-1} for the 500 kHz bandwidth. This was not adequate to resolve the spectral features in most of the sources observed.

The raw data tapes from the VY CMa observations were saved and reprocessed through the new NRAO 288-channel correlator which became available in 1975 March. The resolution for this source was thereby improved to 6.9 kHz or 1.3 km s^{-1}, which was still not really adequate.

The total-power spectra were calculated from the autocorrelation functions of the data on the individual tapes. Fringe visibilities were calculated by dividing the magnitude of the cross-power spectrum for each observation by the geometric mean of the two total-power spectra. For features which had low signal-to-noise ratios, it was necessary to remove a bias in the fringe visibility estimate.

The coherence time of the interferometer was found to be about 10 minutes. This is below normal for this frequency with two hydrogen maser frequency standards and was probably due to the poor operation of the Algonquin maser. The coherence time was extended by choosing a feature in each spectrum to serve as a phase reference. Isolated features without interfering subcomponents were sometimes hard to find, partly because of our inadequate spectral resolution.

A map of the position of the various spectral features, or maser spots, relative to that of the feature used as a phase reference was made for each source by analysis of the relative fringe frequencies. Because so few measurements were taken, lobe ambiguities made the phase information essentially useless. For each velocity channel of each observation, a 32-point Fourier transform of the 25 minute temporal series of cross-power spectra was calculated; this gave a fringe frequency spectrum with a width of 21.3 mHz and a resolution of 0.67 mHz. The fringe frequency of the strongest peak was determined by interpolation. The angular position for each velocity component was then found by fitting the fringe frequencies of the various observations in a least-squares sense to the equation

$$f_{\mathrm{R}} = A[\theta_x \cos(H) + \theta_y \sin \delta_s \sin(H)] . \quad (1)$$

A is 1.3 mHz arcsec^{-1}, H is the hour angle of the source with respect to the hour angle of the baseline, δ_s is the source declination, and θ_x and θ_y are the angular offsets in the right ascension and declination directions, respectively. The nominal 1 σ errors were $\pm 0''.05$ in θ_x and $\pm 0''.05/\sin \delta_s$ in θ_y for an error of 60 μHz in the measurements. The errors found in the solutions to equation (1) were frequently substantially worse than those theoretically expected because of the spectral blending of features due to either insufficient spectrometer resolution or intrinsic feature widths.

One difficulty in making maps from interferometer data involves correctly determining the sign convention of the fringe phase or fringe rate. The wrong sign determination leads to inverted θ_x and θ_y axes. Fortunately, the cluster of H_2O maser spots in Orion A is so extended (Moran *et al.* 1973; Baudry, Forster, and Welch 1974) that the maps produced by the interferometer processing programs can be checked against maps made with single paraboloid antennas, where considerably simpler thought processes determine which way is up. We checked our programs in this and other ways. The maps reported by the Jodrell Bank group (Davies, Masheder, and Booth 1972; and Masheder, Booth, and Davies 1974; both hereafter Jodrell Bank) have axes opposite to ours. We are convinced that ours are correct. In subsequent comparisons between our data and the Jodrell Bank data, we have reversed their axes.

IV. RESULTS

None of the observations of the sources IRC +10011, IRC +50137, OH 1735−32, OH 1821−12, OH 1837−05, OH 1854+02, R Aql, and IRC −20540 produced any measurable signal in the cross-power spectra. The total-power spectra, on the other hand, which were calculated from the individual data tapes, indicated that both antennas were pointed properly and that signals from the sources were properly recorded. The cross-power spectra were searched over a wide range of fringe frequencies to accommodate any reasonable source position errors. Hence we feel confident that these negative results indicate that these sources were resolved. Specific results and lower limits on the sizes and upper limits on the brightness temperatures are given in Table 1. Reid and Muhleman (1975) made VLBI observations with a baseline about half as long as ours, detected weak fringes on R Aql, and determined its size to be $0''.10$. They failed to detect fringes on IRC +10011, IRC +10529, or OH 1837−05. Recent results with even shorter baselines indicated that many other masers associated with long-period variables are larger than $0''.1$ (Reid *et al.* 1977).

All the observations of VY CMa, NML Cyg, VX Sgr, and W43 A produced fringes. The projected baseline or (u, v)-plane coordinates for these four sources are shown in Figure 1, with observation points indicated. The results of the analysis of the data are listed in Table 2. Note that all velocities in this paper

TABLE 1
NEGATIVE RESULTS

Source	Number of Observations	F(Low) (Jy) (1)	F(High) (Jy) (2)	θ(Low) (arcsec) (3)	θ(High) (arcsec) (4)	T_B(Low) (10^{10} K) (5)	T_B(High) (10^{10} K) (6)
IRC +10011	4	20	18	0.04	0.04	0.6	0.5
IRC +50137	1	2	8	0.02	0.03	0.2	0.4
OH 1735−32	2	13	27	0.07	0.08	0.1	0.2
OH 1821−12	3	17	10	0.04	0.03	0.5	0.5
OH 1837−05	3	16	5	0.05	0.06	0.3	0.6
OH 1854+02	4	12	9	0.04	0.04	0.3	0.3
R Aql	5	6	48	0.03	0.05	0.3	0.9
IRC −20540	3	7	4	0.03	0.02	0.4	0.5

NOTE.—Columns (1, 2), flux densities of low- and high-velocity components respectively with 2 km s^{-1} spectral resolution; cols. (3, 4), lower limits on the angular size of low- and high-velocity components, respectively, assuming a Gaussian distribution of brightness. The angle is the full width at half-maximum; and cols. (5, 6), upper limits on the apparent brightness temperatures for the low- and high-velocity components.

TABLE 2
FLUX DENSITIES, VISIBILITIES, AND RELATIVE POSITIONS OF SPECTRAL FEATURES

Velocity* (km s^{-1})	F (Jy)	V_{av}	V_{min}	V_{max}	θ_x† (arcsec)	θ_y† (arcsec)
VY CMa						
+55.6	34	0.09	0.05	0.14	+0.32 ± 0.04	−0.67 ± 0.16
+52.4	116	0.19	0.14	0.30	+0.15 ± 0.05	+0.88 ± 0.20
+49.1	82	0.17	0.13	0.23	−0.08 ± 0.03	+0.74 ± 0.12
+46.5	90	0.18	0.11	0.27	+0.01 ± 0.02	−0.56 ± 0.10
+44.0	82	0.17	0.06	0.22	−0.07 ± 0.05	−0.61 ± 0.26
+42.0	68	0.23	0.17	0.31	−0.35 ± 0.02	+0.47 ± 0.11
+38.1	48	0.30	0.17	0.48	−0.24 ± 0.01	−0.65 ± 0.06
+35.6	20	0.19	0.10	0.25	−0.29 ± 0.03	+0.43 ± 0.11
+4.6	8	1.05	0.83	1.10	0	0
−3.8	78	0.18	0.15	0.22	+0.08 ± 0.05	−0.25 ± 0.20
−5.8	164	0.11	0.08	0.13	−0.22 ± 0.05	+0.48 ± 0.21
−7.7	170	0.14	0.07	0.24	+0.21 ± 0.02	−1.06 ± 0.08
−10.3	188	0.14	0.04	0.31	−0.08 ± 0.01	+0.16 ± 0.06
VX Sgr						
+25.4	58	0.09	0.04	0.14	−0.13 ± 0.20	−0.5 ± 0.7
+19.6	42	0.18	0.05	0.30	+0.09 ± 0.03	+1.4 ± 0.1
+15.7	22	0.13	0.04	0.19	−0.83 ± 0.06	+1.4 ± 0.2
−8.5	28	0.09	0.07	0.11	−0.01 ± 0.15	−1.5 ± 0.5
−14.3	44	0.18	0.05	0.28	0	0
W43 A						
40.3	40	0.22	0.21	0.23	0	0
27.2	16	0.16	0.11	0.33	0.26 ± 0.05	−1.1 ± 1.5
NML Cyg						
+22.2	158	0.05	0.04	0.06	+1.29 ± 0.02	−0.59 ± 0.03
+17.4	50	0.08	0.10	0.05	−0.41 ± 0.30	+0.96 ± 0.35
+7.7	36	0.07	0.06	0.08	−2.01 ± 0.35	+0.24 ± 0.40
−12.6	26	0.11	0.08	0.14	−1.09 ± 0.02	+0.81 ± 0.03
−17.5	188	0.08	0.03	0.12	+0.36 ± 0.10	−0.74 ± 0.12
−23.7	460	0.08	0.03	0.14	−0.03 ± 0.02	−0.05 ± 0.03
−26.2	330	0.07	0.03	0.08	0	0

* With respect to the local standard of rest.

† The errors are formal 1 σ values. A zero entry means that this feature was used as a phase reference.

1977ApJ...211..160M

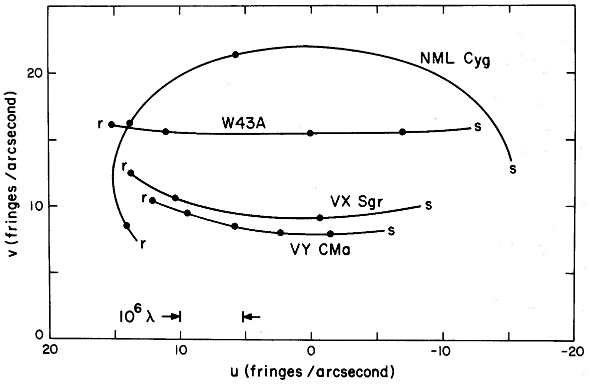

FIG. 1.—Possible (u, v)-plane coverage for the Algonquin Park–NRAO interferometer. (*Dots*), our observations; (*r*), rising; (*s*), setting.

are given with respect to the local standard of rest. The velocity components listed in the table correspond to peaks in the average of all the cross-power spectra. There are certainly more features present in the source spectra, but the spectral resolution of the data processor would not allow more to be clearly identified. The average, minimum, and maximum fringe visibilities based on the ensemble of 25 minute observations are listed for each feature. The errors are estimated to be about 30%. These large error bars are due to the phase stability problems mentioned above. The positions given in the table were determined with respect to the feature used as a phase reference in each source. The errors quoted are formal, 1 σ values.

Table 3 lists the sizes of the maser spots based on the average fringe visibilities. A circularly symmetric Gaussian distribution of brightness was assumed to derive the angular diameters. The diameters should be multiplied by about 1.4 to convert to a source model of uniform brightness distribution. The linear dimensions in Table 3 are based on the source distances given by Masheder, Booth, and Davies (1974), but these distances are uncertain. Table 3 also lists the size of the cluster of maser spots in each source.

V. DISCUSSION OF RESULTS

a) NML Cyg

The OH spectrum toward NML Cyg exhibits the characteristic structure of OH/IR masers with the spectral features confined to two distinct velocity ranges. The spectral structure within the high- and low-velocity ranges is very complex, with many overlapping features. There is no evidence for any substantial change in the spectrum since its discovery in 1968 (Wilson and Barrett 1968). The H_2O maser emission is very weak and occurs over a small velocity interval near -20 km s^{-1}. Our spectra and the map of the principal features are shown in Figures 2 and 3. The apparent angular size obtained in this study agrees with the earlier results of Wilson, Barrett, and Moran (1970). We also confirm the results of Reid and Muhleman (1975) which showed that the features in the low-velocity range have higher visibility than those in the high-velocity range.

The general agreement between our map and the one prepared by the Jodrell Bank group is fairly good. Their map is probably preferable because of its better hour-angle coverage and better spectral resolution. In our map, the velocities of the three high-velocity components (22.2, 17.4, and 7.7 km s^{-1}) decrease from southeast to northwest. The four low-velocity features (-12.6, -17.5, -23.7, and -26.2 km s^{-1}) lie within the perimeter defined by the high-velocity features. The feature with the lowest velocity (-26.2 km s^{-1}) lies close to the center of the map. These characteristics were seen by the Jodrell Bank group in their data and were interpreted by them as evidence that the maser emission comes from a rotating, expanding envelope around the central star. In this model, the low-velocity features come from the part of the envelope in front of the star and the high-velocity features from the tangential points. They deduced a rotational velocity of 5 km s^{-1}, which leads to a mass of 15 $M_\odot$ for the star from consideration of gravitational stability. This is rather large but not unreasonable.

TABLE 3

PARAMETERS OF SOURCES WITH FRINGES

SOURCE	DISTANCE* (pc)	NUMBER OF OBSERVATIONS	SPECTRAL RESOLUTION (km s^{-1})	NUMBER OF FEATURES IDENTIFIED	AVERAGE FEATURE SIZE†		FIELD SIZE		PEAK T_B (10^{10} K)	VELOCITY RANGE OF H_2O MASER (km s^{-1})
					(arcsec)	(10^{14} cm)	(arcsec)	(10^{16}cm)		
VY CMa.....	1500	6	1.3	13	0.06‡	13	2.5	6	2.5	-10, 40
VX Sgr......	1700	3	3.8	5	0.07	18	2.5	7	0.6	-15, 15
W43 A.......	2000	4	1.9	2	0.05	15	1	3	0.7	...
NML Cyg....	500	3	3.8	7	0.04	3	3.5	3	12	-18, -20

* Adopted from Masheder *et al.* (1974).

† Size refers to the full width at half-maximum of a Gaussian brightness model. Multiply by about 1.4 to obtain approximately equivalent size of uniformly bright model.

‡ VY CMa had one feature at 4.6 km s^{-1} which was unresolved and smaller than 0″.02 and had a brightness temperature greater than 10^{10} K.

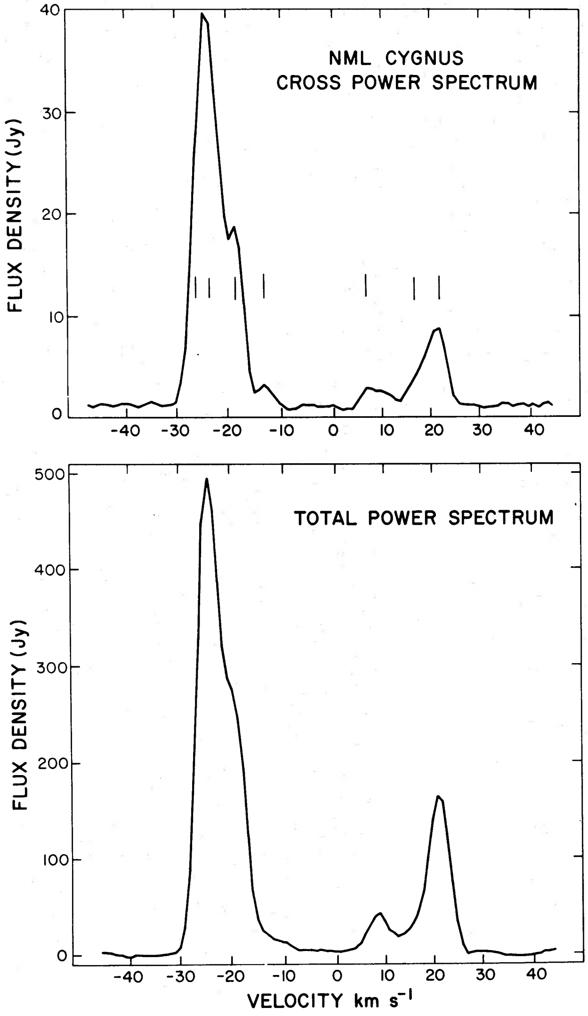

FIG. 2.—Average of the magnitudes of the cross-power spectra (total integration time of 75 minutes) and the geometric mean of the individual total-power spectra (integration time of 4 minutes) for NML Cyg. The spectral resolution is 3.9 km s^{-1}. The Doppler velocity is based on a rest frequency of 1612.231 MHz and is referred to the local standard of rest. The vertical bars mark the velocities of the features whose positions are listed in Table 2.

b) *VY CMa*

The OH spectrum of VY CMa is very complex at the 1612 MHz transition and has changed very little since its discovery in 1969 (Eliasson and Bartlett 1969). On the other hand, the H_2O spectrum generally contains features between -10 and 40 km s^{-1} and has changed dramatically over the last few years. The average cross-power spectrum and the total-power spectrum for our observations are shown in Figure 4. Even with the 288-channel cross-correlator and a resolution of 1.3 km s^{-1}, the features are not well distinguished. To give an impression of the overall extent of the maser emission, we plot in Figure 5 the positions of the emission in all the velocity channels for which the rms error in the least mean-square fit to equation (1) was less than 0.1 mHz (this corresponds to position errors of less than 0″.05 in right ascension and 0″.20 in declination). Only the most reliable positions corresponding to spectral peaks are listed in Table 2. This map can be compared with the one published by the Jodrell Bank group. The gross structure is the same; the angular extent is about 2″.5 with some elongation along a position angle of 160°. There is, perhaps, a tendency for the low-velocity features to cluster toward the center of the masing region. The detailed correspondence of the positions by velocity components is not particularly good. The detailed agreement between our map and that of Reid (1975) made with baselines of 227 and 480 km is quite good.

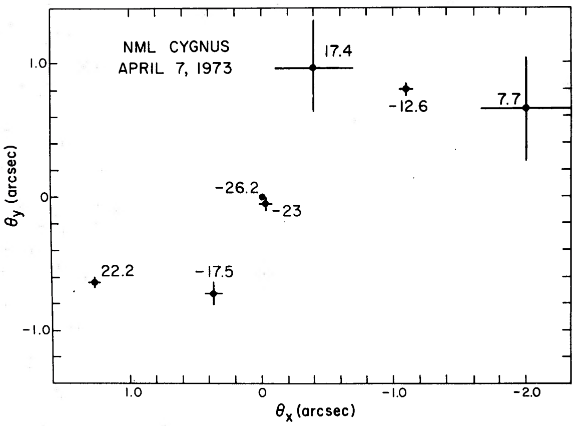

FIG. 3.—Map of the relative positions of the principal features in NML Cyg. The errors are formal 1 σ values, θ_x is in the direction of increasing right ascension, and θ_y is in the direction of increasing declination (*top*, north; *left*, *east*).

The fringe visibilities are generally rather low. Part of the reason is the overlapping of features in velocity. For example, even with a fringe spacing of 1″.6, the Jodrell Bank group observed low apparent visibilities. It is interesting to note that the feature at 4.6 km s^{-1}, which is rather insignificant in the total-power spectrum, appears prominently in the cross-power spectrum and exhibits nearly unity fringe visibility on all projected baselines. It is therefore smaller than 0″.02. Reid (1976) has suggested that this feature, because of its small angular size, may be the amplified image of the stellar continuum radiation field. In this case the star would be directly behind the 4.6 km s^{-1} OH cloud.

c) *VX Sgr*

The H_2O maser toward VX Sgr had features around 0 km s^{-1} and a flux density of only 15 Jy in 1975 February. The velocities of the H_2O features are confined to a narrow range between the two OH velocity ranges. The spectra and map of the OH features are shown in Figures 6 and 7. The visibilities of most of the features increased as a baseline foreshortened, lending support to a single-component model for the brightness distribution.

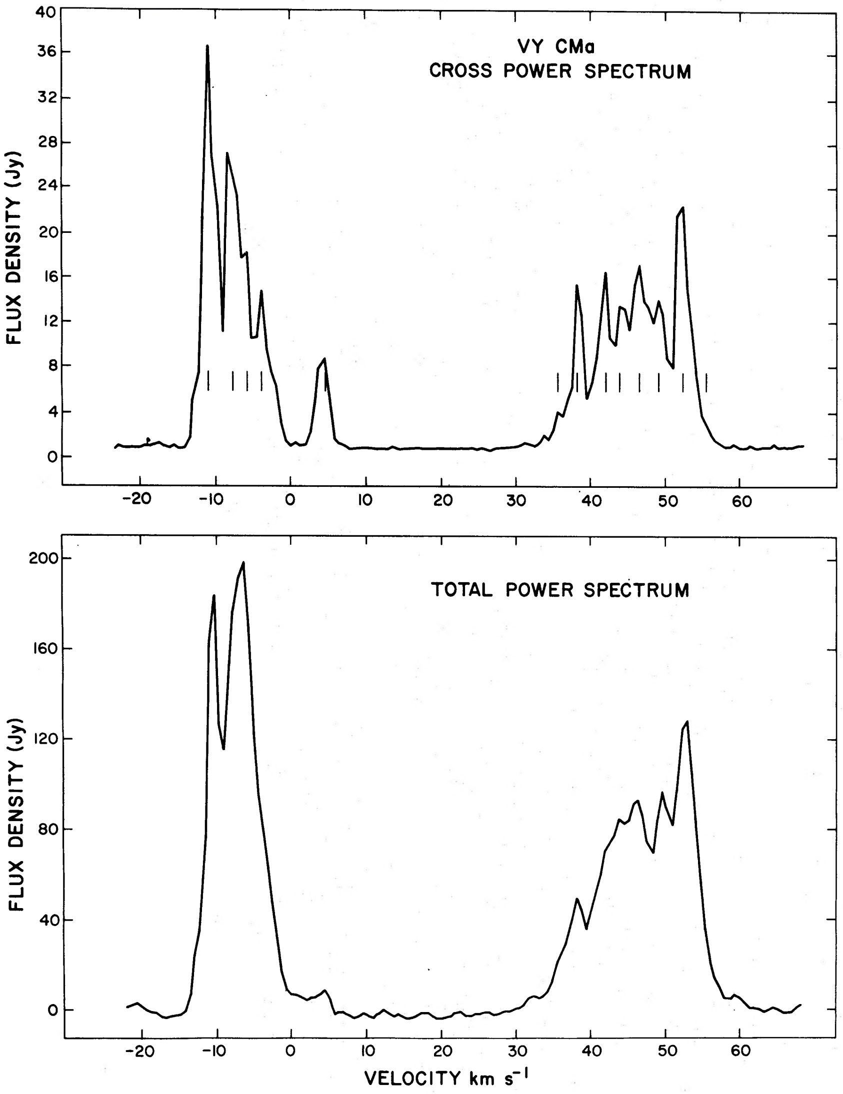

FIG. 4.—Average of the magnitudes of the cross-power spectra (integration time of 150 minutes) and the geometric mean of the total-power spectra (integration time of 4 minutes) for VY CMa. The resolution is 1.3 km s^{-1}.

d) *W43 A*

W43 A had OH emission over the range from 25 to 45 km s^{-1}. No H_2O maser or IR source has been found near this OH maser. The nearby OH and H_2O masers (Yngvesson *et al.* 1975) with velocities of about 90 km s^{-1} are probably associated with the H II region W43 whose recombination line velocity is 97 km s^{-1}. Whether W43 A should be classed with the supergiants or with the long-period variables is not clear. The simplicity of the spectrum and the narrow velocity spread suggest classification with the long-period variables, but the brightness temperatures of the features are more typical of the supergiants. The total-power and cross-power spectra of the OH source are shown in Figure 8. The two strongest features at 40.3 and 27.2 km s^{-1} are separated by about 1″ (see Table 2).

VI. KINEMATIC MODELS

The rotating expanding shell model proposed by the Jodrell Bank group is too complex to be dealt with here in an analytic way, because of the paucity of our data. Instead, we fitted some of our data and some of the Jodrell Bank data to a simple expanding shell model as proposed by Herbig (1974) to explain the maser map of NML Cyg. In this model, the OH spots are assumed to originate from points on a thin spherical shell which is expanding radially away from the star. The model has five parameters: θ_{x_0} and θ_{y_0}, the coordinates of the center of expansion,

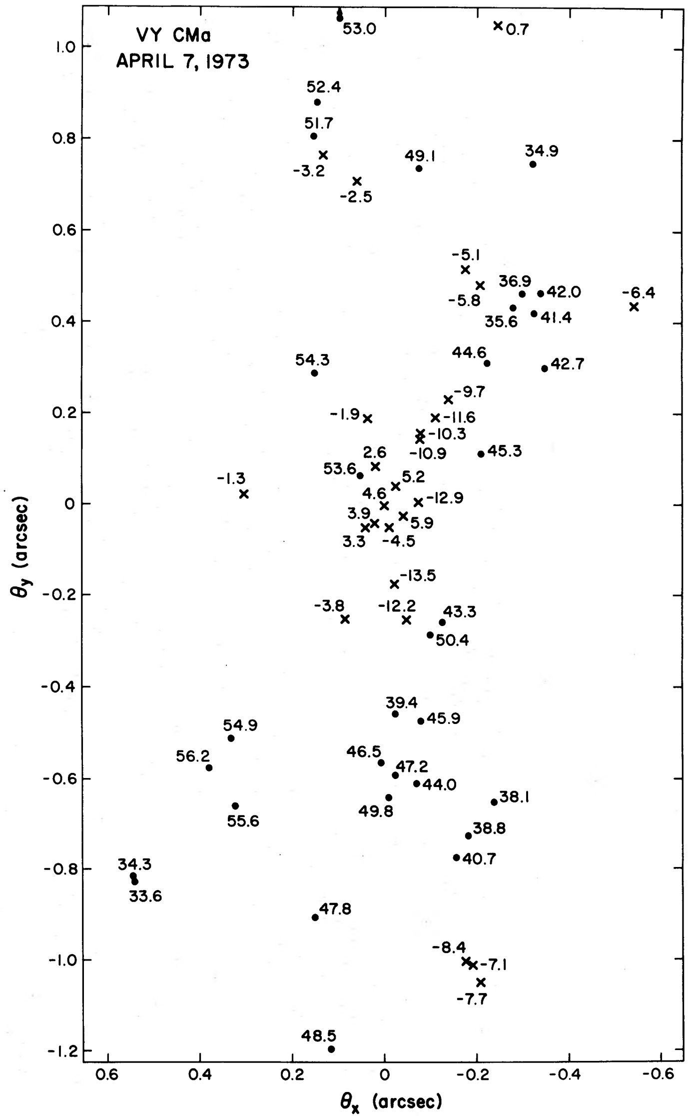

FIG. 5.—Map of relative positions of all velocity components in VY CMa for which the mean-square error in the fit to eq. (1) is less than 0.1 mHz. The positions of features with velocities in the low-velocity part of the spectrum are plotted with the symbol (×) and those in the high-velocity part with the symbol (•).

which presumably are the stellar coordinates; V_0, the Doppler velocity of the star with respect to the local standard of rest; V_E, the expansion velocity of the shell; and R, the radius of the shell. The velocity of the ith maser spot is

$$V_i = V_0 - V_E \cos \psi_i \,, \qquad (2)$$

where ψ_i is the polar angle between the line of sight to the observer and the ith maser spot as seen from the star. The projected distance from the star to the ith maser spot is then

$$d_i = R\left[1 - \left(\frac{V_i - V_0}{V_E}\right)^2\right]^{1/2} \qquad (3)$$

Solutions were sought which minimized the mean-square error between the projected distances of the spots in the model as given in equation (3) and the data. In order to find all the local minima in this nonlinear problem, we wrote a simple computer program to calculate the mean-square error as the five model parameters were varied. All the data were weighted equally, regardless of the flux density, position uncertainty, or velocity width of the features. Models for which the square root in equation (3) was negative for any maser spot were excluded. In this manner more than 10^5 sets of parameters were inspected for the maps of NML Cyg and VY CMa. The parameters for the models with the lowest errors are listed in Table 4.

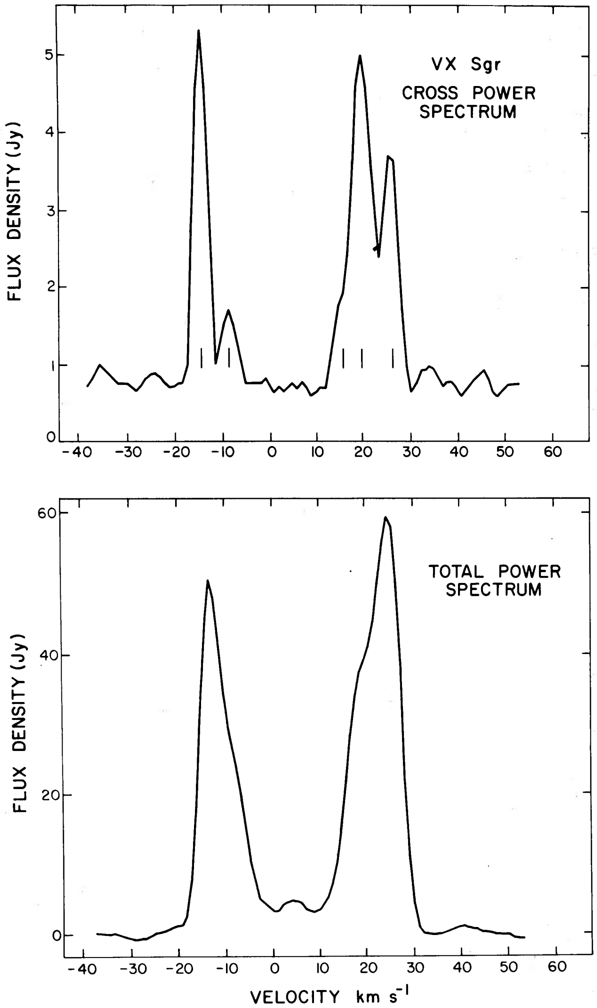

FIG. 6.—Average of the magnitudes of the cross-power spectra (integration time of 75 minutes) and the geometric mean of the total-power spectra (integration time of 4 minutes) for VX Sgr. The resolution is 3.9 km s^{-1}.

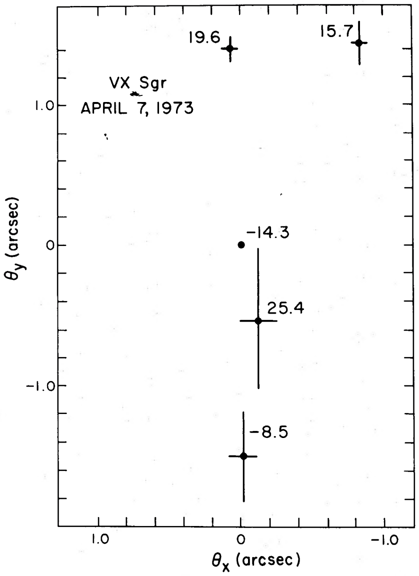

FIG. 7.—Map of the relative positions of the principal features in VX Sgr.

The data from the NML Cyg maps presented here and by the Jodrell Bank group (as selected by Herbig 1974) were searched over the following range of parameters: $\theta_{x_0}(-5'', 5'')$, $\theta_{y_0}(-5'', 5'')$, $V_0(-36, 36$ km s$^{-1})$, $V_E(30, 100$ km s$^{-1})$, and $R(0''.5, 5''.0)$. Only one solution was found for the Jodrell Bank data. The parameters agree pretty well with those found by Herbig (1974). No significant minima in the mean-square error were found for our data on NML Cyg. The error steadily decreased as V_0 was increased beyond 36 km s^{-1}. The solution with V_0 constrained to equal 18 km s^{-1} is given in Table 4 and agrees closely with the parameters for the Jodrell Bank map. With V_0 near the high-velocity end of the spectrum, most of the spots are in the hemisphere facing the Earth. We also give the best model for V_0 constrained to be -3 km s^{-1}, the mean velocity of the OH emission.

TABLE 4

PARAMETERS FOR THE EXPANDING SPHERICAL SHELL MODELS

Source	N (1)	V_0 (km s^{-1}) (2)	V_E (km s^{-1}) (3)	R (arcsec) (4)	θ_{x0} (arcsec) (5)	θ_{y0} (arcsec) (6)	σ (arcsec) (7)	t (years) (8)	f (9)
NML Cyg*.......	6	+18 ± 3	44 ± 3	1.5 ± 0.3	−0.4 ± 0.2	+0.3 ± 0.2	0.15	82 ± 25	0.3
NML Cyg†.......	7	+18	49 ± 4	1.6 ± 0.3	−0.5 ± 0.3	−0.4 ± 0.3	0.19	80 ± 25	0.5
NML Cyg‡.......	7	−3	51 ± 7	1.6 ± 0.5	−0.8 ± 0.3	−0.8 ± 0.3	0.38	75 ± 40	0.5
VY CMa§........	13	+21 ± 5	73 ± 5	4.2 ± 0.5	+3.8 ± 0.4	+0.5 ± 0.4	0.11	420 ± 50	0.04

NOTE.—Column (1), number of maser spots used in analysis; col. (2), velocity of star with respect to local standard of rest; col. (3), expansion velocity of shell; col. (4), shell radius; cols. (5, 6), coordinates of center of expansion with respect to the +4.6 km s^{-1} feature in VY CMa and the 26 km s^{-1} feature in NML Cyg; col. (7), the mean-square error; col. (8), age of shell based on distances of 1500 pc for VY CMa and 500 pc for NML Cyg; col. (9), the fraction of the shell occupied by maser spots.

* Parameters for the data of Davies, Masheder, and Booth (1972) as selected by Herbig (1974).

† Our data (Table 2) with V_0 constrained to be 18 km s^{-1}.

‡ Our data with V_0 constrained to be -3 km s^{-1}.

§ Our data (see Table 2).

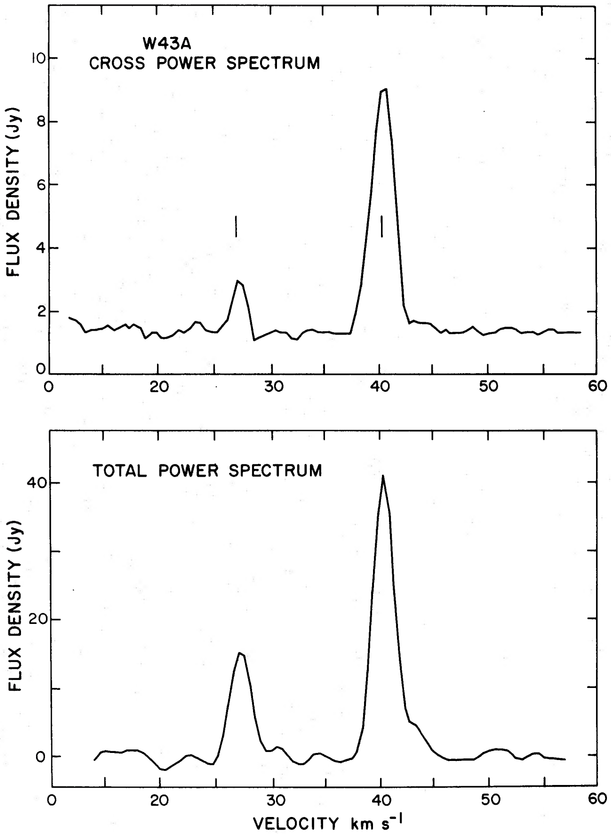

FIG. 8.—Average of the magnitudes of the cross-power spectra (integration time of 100 minutes) and the geometric mean of the total-power spectra (integration time of 4 minutes) for W43 A. The resolution is 1.9 km s^{-1}.

The data on VY CMa were searched over the range of parameters $\theta_{x_0}(-5'', 5'')$, $\theta_{y_0}(-5'', 5'')$, $V_0(-20, 60\ \mathrm{km\ s^{-1}})$, $V_E(30, 120\ \mathrm{km\ s^{-1}})$, and $R(0''.5, 5''.0)$. No significant minima were found for a solution involving the 25 strongest features from the Jodrell Bank map. In a separate solution fitting our data, the 13 positions in Table 2 were used. One minimum was found; its parameters are listed in Table 4. They show the star to be located about 4″ east of the OH maser spots and to have a velocity of 21 km s^{-1}, which is midway between that of the high-velocity and that of the low-velocity OH spots. The model is sketched in Figure 9. This solution arises from the westerly progression of the positions of the spots in the high-velocity group as the velocity decreases. All the features are very near the tangential point of the sphere as viewed from the Earth and occupy a very small part of the shell. For any reasonable stellar mass, the OH exceeds the escape velocity and is being ejected from the system.

The stellar velocity from this model, 21 km s^{-1}, does not agree with the traditional value of about 50 km s^{-1}. However, Reid and Dickinson (1976) have analyzed the thermal SiO emission from several IR stars and found that the mean velocity falls between the two velocity ranges of the OH emission. In particular, they found the velocity for the emission in VY CMa to be 17.5 km s^{-1}, and they suggest that this is the stellar velocity. Furthermore, recent optical data on VY CMa (Humphreys 1975; Wallerstein 1976) strengthen the earlier idea of Herbig (1969) that the stellar velocity is centrally located between the OH peaks at around 20 km s^{-1}.

If the OH spots are plotted on the optical map of the VY CMa nebula (Herbig 1972, Fig. 4), using the center of expansion for the stellar coordinates, then the OH emission lies in an interesting part of the nebula where the optical polarization is large. The radius of the nebula is approximately 4″. However, this large separation between OH and star seems somewhat unlikely, in view of other interferometer measurements. There is some suggestion that the H_2O features (Baudry, Forster, and Welch 1974) and the OH features (Mader 1975) are offset from the stellar position by 1″.5 in a northeasterly direction, which is directly opposite the offset from the thin shell model. Future measurements of the angular offset between the star and OH emission will be needed to definitely rule out this model.

VII. CONCLUSION

The maps of the four OH maser sources NML Cyg, VY CMa, VX Sgr, and W43 A agree well in overall character but not too well in detail with those made by the Jodrell Bank group. Their coordinate axes are probably inverted. In 1973 April, the brightness temperatures of most of the maser features in these four sources were typically 10^{10} K. Only one feature, at 4.6 km s^{-1} in VY CMa, was unresolved and smaller than 0″.02. The linear sizes of these OH/IR features are larger than those of OH features associated with H II regions. Of these sources, only VY CMa has been mapped at the H_2O line frequency of 22 GHz. The H_2O emission spots are smaller than 0″.003 and confined to an area of about 0″.2 in diameter (Moran *et al.* 1973; Moran *et al.* 1976). Hence, both the spot size and the cluster size are about an order of magnitude smaller for the H_2O maser than for the OH maser at 1612 MHz. However, the size of the H_2O cluster of spots toward VY CMa is about the same as the size of the OH cluster at 1665 MHz (P. J. Harvey *et al.* 1974).

Our attempt to fit a model of an expanding shell to the available data for NML Cyg and VY CMa had limited success. This model might serve to provide an approximate kinematic picture of the OH distribution. The probable presence of turbulent motion and other shells of different radii limits its usefulness.

The OH features associated with long-period variables have angular sizes greater than 0″.05 and are best studied with interferometers having baselines between 20 and 200 km.

This program benefited greatly from our discussions with Mark Reid, Marvin Litvak, and Kenneth Bechis. Radio Astronomy at Harvard College Observatory is funded in part by grant MPS 75-05011 from the US National Science Foundation. We thank Haystack Observatory for the loan of their parametric amplifier.

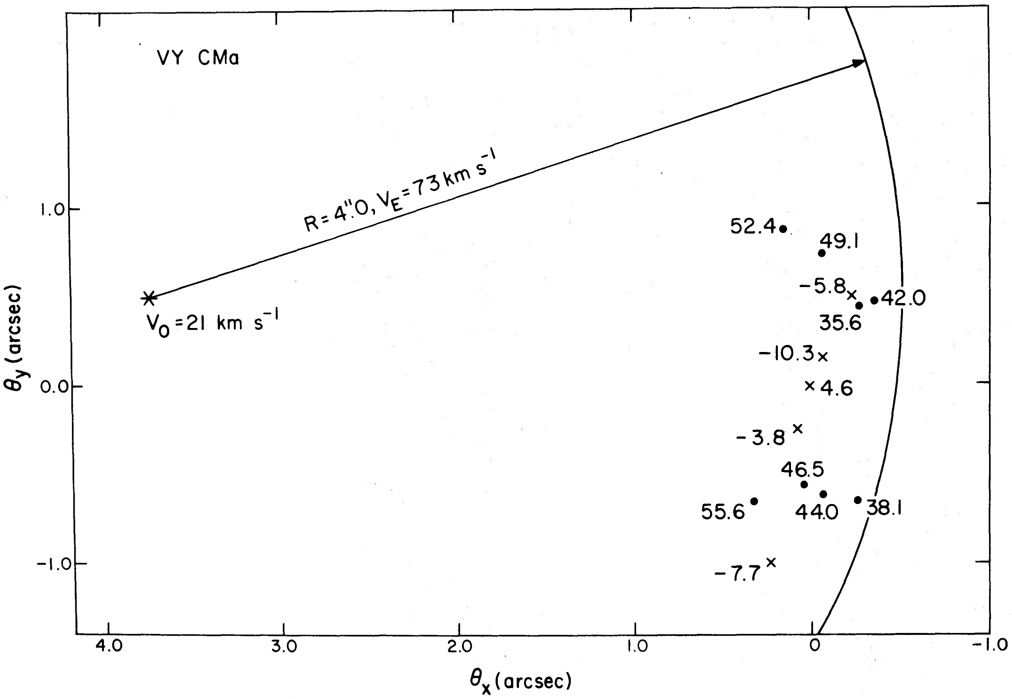

FIG. 9.—Map of the positions of the 13 principal features in VY CMa showing the expansion center and edge of the best-fitting thin shell model.

REFERENCES

Baudry, A., Forster, J. R., and Welch, W. J. 1974, *Astr. Ap.*, **36**, 217.

Clark, B. G. 1973, *Proc. Inst. Elec. Electron. Engrs.*, **61**, 1242.

Davies, R. D., Masheder, M. R. W., and Booth, R. S. 1972, *Nature Phys. Sci.*, **237**, 21 (Jodrell Bank).

Eliasson, B., and Bartlett, J. F. 1969, *Ap. J. (Letters)*, **155**, L79.

Harvey, P. J., Booth, R. S., Davies, R. D., Whittet, D. C. B., and McLaughlin, W. 1974, *M.N.R.A.S.*, **169**, 545.

Harvey, P. M., Bechis, K. P., Wilson, W. J., and Ball, J. A. 1974, *Ap. J. Suppl.*, **27**, 331.

Herbig, G. H. 1969, *Mém.* [8°] *Soc. Roy. Sci. Liège*, p. 13.

———. 1972, *Ap. J.*, **172**, 375.

———. 1974, *Ap. J.*, **189**, 75.

Humphreys, R. M. 1975, *Pub. A.S.P.*, **87**, 433.

Mader, G. L. 1975, Ph.D. thesis, University of Maryland.

Masheder, M. R. W., Booth, R. S., and Davies, R. D. 1974, *M.N.R.A.S.*, **166**, 561 (Jodrell Bank).

Moran, J. M. 1973, *Proc. Inst. Elec. Electron. Engrs.*, **61**, 1236.

Moran, J. M., Johnston, K. J., Walker, R. C., and Burke, B. F. 1976, in preparation.

Moran, J. M., Papadopoulos, G. D., Burke, B. F., Lo, K. Y., Schwartz, P. R., Thacker, D. L., Johnston, K. J., Knowles, S. H., Reisz, A. C., and Shapiro, I. I. 1973, *Ap. J.*, **185**, 535.

Reid, M. J. 1975, Ph.D. thesis, California Institute of Technology.

———. 1976, private communication.

Reid, M. J., and Dickinson, D. F. 1976, *Ap. J.*, **209**, 505.

Reid, M. J., and Muhleman, D. O. 1975, *Ap. J. (Letters)*, **196**, L35.

Reid, M. J., Muhleman, D. O., Moran, J. M., Johnston, K. J., and Schwartz, P. R. 1977, *Ap. J.*, in press.

Wallerstein, G. 1976, private communication.

Wilson, W. J., and Barrett, A. H. 1968, *Science*, **161**, 778.

———. 1972, *Astr. Ap.*, **17**, 385.

Wilson, W. J., Barrett, A. H., and Moran, J. M. 1970, *Ap. J.*, **160**, 545.

Yngvesson, K. S., Cardiasmenos, A. G., Shanley, J. F., Rydbeck, O. E. H., and Elldér, J. 1975, *Ap. J.*, **195**, 91.

J. A. BALL: Harvard College Observatory, Harvard, MA 01451

K. J. JOHNSTON: Code 7134, E. O. Hulburt Center for Space Research, Naval Research Laboratory, Washington, DC 20375

S. H. KNOWLES: Code 7132, E. O. Hulburt Center for Space Research, Naval Research Laboratory, Washington, DC 20375

J. M. MORAN: Center for Astrophysics, Harvard College Observatory and Smithsonian Astrophysical Observatory, 60 Garden Street, Cambridge, MA 02138

P. R. SCHWARTZ: Code 7138, E. O. Hulburt Center for Space Research, Naval Research Laboratory, Washington, DC 20375

J. L. YEN: Department of Electrical Engineering, University of Toronto, Toronto, Ontario, Canada